

# Formation of ZnO thin films by photocatalytic reaction

Hiromasa Nishikiori,<sup>1,\*</sup> Satoshi Nagaya,<sup>2</sup> Takumi Takikawa,<sup>1</sup> Ayaka Kikuchi,<sup>1</sup> Tomohiko

Yamakami,<sup>1</sup> Hajime Wagata,<sup>1</sup> Katsuya Teshima,<sup>1</sup> Tsuneo Fujii<sup>3</sup>

<sup>1</sup> Faculty of Engineering, Shinshu University, 4-17-1 Wakasato, Nagano 380-8553, Japan

<sup>2</sup> Nagano Prefecture General Industrial Technology Center, 1-3-1, Osachi-Katamacho, Okaya,  
Nagano 394-0084, Japan

<sup>3</sup> Nagano Prefectural Institute of Technology, 813-8 Shimonogo, Ueda, Nagano 386-1211,  
Japan

Corresponding author: Hiromasa Nishikiori

Tel: +81-26-269-5536

Fax: +81-26-269-5531

E-mail: [nishiki@shinshu-u.ac.jp](mailto:nishiki@shinshu-u.ac.jp)

## **Abstract**

Zinc oxide and layered zinc hydroxides were deposited from an aqueous solution of zinc nitrate at 323–358 K on a substrate plate with a very thin titanium dioxide film by a photocatalytic reaction. The amorphous or low crystalline zinc hydroxide aggregates were deposited at a low temperature. The zinc oxide crystals with about 1–2  $\mu\text{m}$ -sized hexagonal columns and 10 nm-sized spheres were formed at 338–358 K. Nitrate ions in the solution were reduced to nitrite ions, and water was transformed into hydroxide ions by a photocatalytic reaction on the titanium dioxide film. The pH value increased on the substrate surface with the titanium dioxide film, which caused the zinc hydroxide formation on the film. The zinc hydroxides were then dehydrated and transformed into zinc oxide. The average crystallite size of the zinc oxide decreased with an increase in the reaction temperature because the reaction rates of the formation and dehydration of the zinc hydroxides increased which resulted in an increase in the formation rate of the crystal zinc oxide nuclei.

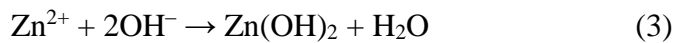
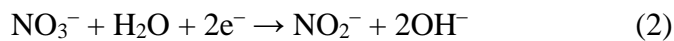
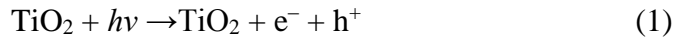
**Keywords:** Zinc Oxide; Layered Zinc Hydroxide; Photocatalytic Reaction; Titanium Dioxide

## 1. Introduction

Zinc oxide (ZnO) as well as titanium dioxide (TiO<sub>2</sub>) possess a semiconductor property and function as photocatalysts [1–3]. The ZnO semiconductor electrodes are widely investigated for application in dye-sensitized solar cells because they exhibit a high bulk electron mobility [2]. ZnO films used to be prepared by radio frequency magnetron sputtering and chemical vapor deposition. In the 1990s, electrodeposition was invented by Izaki [4] and Lincot [5,6] and has been investigated as a low temperature process. During the electrodeposition process, ZnO films were formed in an aqueous solution of zinc nitrate (Zn(NO<sub>3</sub>)<sub>2</sub>) or zinc chloride (ZnCl<sub>2</sub>).

The ZnO films are also prepared by an electroless deposition or chemical reaction instead of electrodeposition, which can be used to synthesize various materials because it does not require electrically conductive substrates [7,8]. Such methods can easily prepare films consisting of nanosized particles that have a high specific surface area due to the slow deposition rate. Izaki prepared ZnO films by a chemical reaction or a light-assisted chemical reaction of a solution containing Zn(NO<sub>3</sub>)<sub>2</sub> and dimethylamine–borane [9,10]. However, these methods require very strong reductants of the boranes and cause a small amount of boron to remain in the films. We tried to prepare ZnO films utilizing the photocatalytic function of TiO<sub>2</sub> instead of such reductants.

In a previous study, ZnO particles were deposited on a very thin TiO<sub>2</sub> film by a photocatalytic reaction of TiO<sub>2</sub> [11]. The formation process of the ZnO can be expressed as follows [12–14]:



Upon light irradiation at a wavelength shorter than ca. 390 nm, TiO<sub>2</sub> is excited resulting in the charge separation of electrons and holes because the band gap of anatase TiO<sub>2</sub> is ca. 3.2 eV (Eq. 1). On the surface on the film, the nitrate ions in the solution are reduced to nitrite ions, and water is transformed into hydroxide ions (Eq. 2). The pH value increased on the TiO<sub>2</sub> surface, which caused the zinc hydroxide (Zn(OH)<sub>2</sub>) formation on the film (Eq. 3). The Zn(OH)<sub>2</sub> was then dehydrated and transformed into ZnO (Eq. 4). The particles were formed in an aqueous solution of Zn(NO<sub>3</sub>)<sub>2</sub> at 343K. The particles consisted of crystals with 0.20–1.0 μm-sized hexagonal columns. A photocurrent was observed in the electrodes containing such ZnO crystals during light irradiation. However, nanocrystalline particles are required for the photocatalytic photovoltaic electrodes, such as dye-sensitized solar cells, due to their high specific surface area. In this study, the films consisting of ZnO nanoparticles were prepared

on the substrate plate with a TiO<sub>2</sub> thin film by the photocatalytic reaction. We will discuss the influence of the reaction conditions on the microscopic morphology of the deposited particles and the mechanism of their formation based on the surface analyses of the samples.

## **2. Experimental**

### **2.1 Materials**

Hydrated zinc nitrate (Zn(NO<sub>3</sub>)<sub>2</sub>·6H<sub>2</sub>O), titanium tetraisopropoxide, ethanol, 2-propanol, diethyleneglycol, polyethyleneglycol (M.W. = 20,000), nitric acid, hydrochloric acid, sodium hydroxide, tin (II) chloride, silver nitrate, and palladium (II) chloride (Wako, S or reagent grade) were used without further purification. Water was ion-exchanged and distilled by a distiller (Yamato WG23). The glass plate (Matsunami S-1111) and ITO glass plate (AGC Fabritech, 14 Ω cm<sup>-2</sup>) were used after washing with ethanol.

### **2.2 Sample Preparation**

Aqueous solutions of 0.10, 0.30, and 0.50 mol dm<sup>-3</sup> Zn(NO<sub>3</sub>)<sub>2</sub>·6H<sub>2</sub>O were prepared with water and sodium hydroxide in which the pH value was ca. 6. The glass substrates were coated with a very thin TiO<sub>2</sub> film by the sol–gel method. The sol was prepared by mixing 25.0 cm<sup>3</sup> of ethanol, 0.21 cm<sup>3</sup> of nitric acid, and 0.21 cm<sup>3</sup> of water and then adding 5.0 cm<sup>3</sup> of titanium tetraisopropoxide in a dry nitrogen atmosphere. The anatase-type TiO<sub>2</sub> films were

prepared by three or ten dip-coatings using the sol and then heating at 773K for 30 min. The thickness of the three- or ten-layered film was ca. 50 or 150 nm, respectively.

The substrates with the TiO<sub>2</sub> film were rinsed in 2-propanol and 0.10wt% polyethyleneglycol aqueous solutions along with ultrasonication for 5 min each. Furthermore, they were rinsed in water with ultrasonication for 1 min, then immersed in 1.0 mol dm<sup>-3</sup> hydrochloric acid containing 0.24 mol dm<sup>-3</sup> SnCl<sub>2</sub> as the sensitizer, 4.4 mmol dm<sup>-3</sup> AgCl as the first activator, and 5.9 mmol dm<sup>-3</sup> PdCl<sub>2</sub> as the second activator for 10 min each [15,16]. Sn<sup>2+</sup> was adsorbed on the substrate surface, and then substituted with Ag and Pd because Sn<sup>2+</sup> reduced Pd<sup>2+</sup>. Consequently, Ag and Pd particles were formed on the surface as the nuclei for the ZnO crystal growth and as the promoter for the TiO<sub>2</sub> photocatalyst. The substrates were immersed in the Zn(NO<sub>3</sub>)<sub>2</sub> solution maintained at 323–358 K in the dark or during light irradiation using a high-pressure mercury lamp (SEN LIGHTS HB-100-A, 100 W) without stirring. The distance between the substrate and lamp was ca. 2 cm. After the irradiation for 2 h, the samples were washed with water, then dried at room temperature.

### 2.3. Measurements

Micromorphology of the samples was done using a field emission scanning electron microscope (FE-SEM, Hitachi SU8000), scanning transmission electron microscope (STEM, Hitachi HD-2300A), and transmission electron microscope (TEM, JEOL JEM-2010). The

elemental mapping and elemental composition analysis were conducted by an electron probe microanalyzer (EPMA, Shimadzu EPMA-1610) and energy-dispersive X-ray spectroscope (EDS, Hitachi HD-2300A). The X-ray diffraction patterns were obtained using an X-ray diffractometer (XRD, Rigaku SmartLab). The UV-vis absorption spectra were measured using a spectrophotometer (Shimadzu UV-3150). For examination of the photocatalytic properties, the substrates with an ITO film were coated with TiO<sub>2</sub> on which the ZnO particles were deposited by the method described above. The electrolyte solution consisting of diethyleneglycol containing 0.50 mol dm<sup>-3</sup> LiI and 50 mmol dm<sup>-3</sup> I<sub>2</sub> was allowed to soak into the space between the sample and the counter Pt electrode. The samples were irradiated with monochromatic light generated by a fluorescence spectrophotometer (Shimadzu RF-5300) using a Xe short arc lamp. During the light irradiation, the short circuit current was measured in the range from 350 to 400 nm by a digital multimeter (ADC 7461A). The samples without ZnO were used as references.

### **3. Results and Discussion**

#### **3.1 Microscopic morphology of the sample surface**

The samples were prepared on the substrate plates coated with the three-layered TiO<sub>2</sub> for microscopic morphology observation. The SEM image and Raman spectrum of the surface of

the three-layered TiO<sub>2</sub> film are shown in Figures S1 and S2, respectively (Supplementary information). The TiO<sub>2</sub> film consisted of ca. 20-nm-sized particles. The Raman spectrum corresponded to that of the anatase-type TiO<sub>2</sub> standard. No XRD peak was detected on the substrate due to the thinness of the layer. Figure 1 shows the secondary electron images by SEM observations of the sample surface prepared on the substrate plates at 323–358 K. No particle was deposited on the substrates at each temperature in the dark or on the glass plates without the TiO<sub>2</sub> film even during the light irradiation. Island-like deposits larger than 1 μm were observed in the sample prepared at 323 K. The 1–2-μm-sized particle-like deposits with a blurry outline were observed in the sample prepared at 338 K. The particles consisting of crystals with 1–2-μm-sized hexagonal columns were clearly found in the sample prepared at 348 K. A greater number of hexagonal crystals were found on the sample prepared at 358 K although the particle size was smaller than that in the sample prepared at 348 K.

### Figure 1

Figure 2 shows the XRD patterns of the sample prepared at 323–358 K. The sample prepared at 323 K exhibited a halo peak due to the substrate and weak peak at 9.2° ( $d = 0.96$  nm) assigned to the (200) planes of Zn<sub>5</sub>(OH)<sub>8</sub>(NO<sub>3</sub>)<sub>2</sub>·6H<sub>2</sub>O, i.e., layered zinc hydroxide (LZH) nitrate [17–20]. LZH nitrate is a zinc hydroxide containing nitrate ions between its interlayers and precipitated in a zinc nitrate solution under basic conditions. A weak peak was



also observed at  $10.3^\circ$  ( $d = 0.86$  nm), which can be assigned to the LZH nitrite. This is because the spacing of the (200) plane was reduced by the photocatalytic reduction from  $\text{NO}_3^-$  to  $\text{NO}_2^-$ , the ionic radii of which were ca. 0.20 and 0.16 nm, respectively [21,22]. The island-like deposits as seen in the SEM image (Fig. 1a) can consist of the LZHs. The amorphous or low crystalline LZH aggregates were deposited at a low temperature. Peaks were clearly observed at  $31.7$ ,  $34.3$ ,  $36.2$ ,  $47.4$ , and  $56.5^\circ$  from the sample prepared at higher than 323 K, which were assigned to the (100), (002), (101), (102), and (110) planes of wurtzite ZnO. The relative amount of the ZnO crystals estimated from the (101) peak intensity was 1, 1.3, and 7.8 for the samples prepared at 338, 348, and 358 K, respectively. These results indicate that the light irradiation caused the photocatalytic formation of zinc hydroxide on the  $\text{TiO}_2$  film, and then the heat mainly promoted its dehydration and transformation into ZnO. A peak was also observed at  $38.1^\circ$  assigned to the (111) plane of Ag, which formed nanocrystals. The sample prepared at 338 K consisted of LZHs and ZnO, which formed the particles with a blurry outline as seen in the SEM image (Fig 1b). The LZHs were completely dehydrated and formed ZnO at 348 K. The particle size of the sample prepared at 358 K was smaller than that of the sample prepared at 348 K as shown in the SEM images (Figs. 1c and 1d). This result indicated that the formation rate of the crystal nuclei of ZnO was faster at the higher temperature because the formation rate of the crystal nuclei of the LZHs

and its dehydration rate were faster.

## Figure 2

The average ZnO crystallite sizes of the samples estimated from the full width at half maximum of the (101) peak using Scherrer's equation were 50.4, 35.7, and 29.6 nm for the samples prepared at 338, 348, and 358 K, respectively. The sizes were consistent with the difference in the formation rate of the ZnO crystal nuclei. However, the crystallite sizes (nano size) did not correspond to the particle sizes (micro size) estimated from the SEM images. This fact indicated that the nanocrystals can exist on the substrates although they were not observed by the SEM. The XRD patterns were significantly influenced by the nanocrystals.

The elemental composition and elemental mapping on the sample surface ( $250 \times 250 \mu\text{m}$ ) were obtained by the electron probe microanalyzer (EPMA). The Zn amount relative to Ti was 0.20, 7.3, 8.1, and 24 for the samples prepared at 323, 338, 348, and 358 K, respectively. Figure 3 shows the EPMA mapping images of the sample prepared at 348 K. Zn and O atoms were uniformly observed over the field, indicating that ZnO was distributed over not only the islanded micro-sized particles, but also the substrate surface. The Ag nanocrystals detected by the XRD analysis were aggregated and the size of the resulting particles was less than ca. 10  $\mu\text{m}$ . Pd was uniformly dispersed on the substrate surface as small particles, which were not observed by the XRD analysis.

### **Figure 3**

Figure 4 shows the SEM reflection electron images on the surface and the cross section of the sample prepared at 348 K. A difference in the atomic number of the constituent element reflects the contrast of the image, i.e., the heavier atoms are lighter in the image. The substrate surface apart from the micro-sized ZnO particles was as light as the parts of the micro-sized ZnO particles. However, the parts around the micro-sized ZnO particles were dark, indicating that the lighter atom, i.e., Ti, on the substrate was observed due to lack of Zn atoms. It is suggested that the Zn atoms in this area were used for the micro-sized crystal formation. The cross section image of the sample indicated that the very thin layer exhibited the same contrast as that of the microcrystal on the 50-nm thick TiO<sub>2</sub> thin layer. This part consists of the ZnO nano-sized particles based on the XRD analysis.

### **Figure 4**

Figure 5 shows the EDS mapping images of the STEM for the microcrystal and thin film parts of the sample prepared at 348 K. The Z-contrast images of the microcrystal part indicated that the very thin layer exhibited the same contrast as that of the microcrystal on the thin TiO<sub>2</sub> layer. The Zn mapping image confirmed that the microparticle consisted of Zn atoms. Ag and Pd aggregates were on the microcrystal surface. Therefore, the microcrystals can be formed on the parts of which the Ag and Pd particles were aggregated. The images at

the thin film part indicated that a very thin layer containing Zn, Ag, and Pd was formed on the ca. 50-nm thick TiO<sub>2</sub> layer. This result was consistent with the formation of the ZnO nanocrystal formation. No particle containing Zn was deposited on the substrates in the dark or on the glass plates without the TiO<sub>2</sub> film even during the light irradiation. Figure S3 shows the energy-dispersive X-ray spectrum of the sample's thin film parts. Zinc and titanium were clearly detected on the surface (Supplementary information). Small amounts of Ag and Pd were also found on the substrate.

### **Figure 5**

Figure 6 shows the TEM image of the sample's cross section prepared at 348 K. It indicated that the ca. 20-nm thin layer consisting of ca. 10-nm particles was formed on the ca. 50-nm thick TiO<sub>2</sub> layer. These particles should be the ZnO nanocrystals. The number and volume of the Ag and Pd particles were much lower than those of ZnO because their XRD patterns were weak or not clearly observed.

### **Figure 6**

## **3.2 Photoelectric conversion property**

The photoelectric conversion property of the samples was examined in order to confirm their semiconductor and photocatalytic properties. Figure 7 shows the UV-vis absorption and incident photon-to-current conversion efficiency (IPCE) spectra of the samples prepared at

323–358 K. The absorption spectrum of the ITO glass plate is also shown. This indicated that the absorption of the samples was significantly caused by the ITO layer. The surface morphology of the samples did not change during the photocurrent measurement. The sample prepared at 323 K exhibited a spectrum having the onset at 380 nm although it contained no ZnO based on its XRD pattern. This photocurrent resulted from the TiO<sub>2</sub> layer on the substrate. The IPCE values for the samples increased with the reaction temperature. The increase in the photocurrent corresponded to the amount of the ZnO crystals. The ZnO crystals exhibited a semiconductor property for use as a photovoltaic electrode. The low IPCE values were because the ZnO layer was very thin and the light transmittance was very high.

### Figure 7

### 3.3 Mechanism of ZnO formation

The samples were prepared under specific preparation conditions in order to determine the mechanism of the ZnO formation. Figure 8 shows the SEM images of the samples prepared from the 0.30 and 0.50 mol dm<sup>-3</sup> Zn(NO<sub>3</sub>)<sub>2</sub> solutions on the three-layered TiO<sub>2</sub> and the sample prepared from the 0.10 mol dm<sup>-3</sup> Zn(NO<sub>3</sub>)<sub>2</sub> solution on the ten-layered TiO<sub>2</sub>. Island-like deposits were observed in the sample prepared from the 0.30 mol dm<sup>-3</sup> Zn(NO<sub>3</sub>)<sub>2</sub> solution. Sheet-like flakes were observed in the sample prepared from the 0.50 mol dm<sup>-3</sup> Zn(NO<sub>3</sub>)<sub>2</sub> solution. These results indicated that an increase in the Zn(NO<sub>3</sub>)<sub>2</sub> concentration promoted the

LZH formation and inhibited the LZH dehydration and ZnO formation. The particles with a blurry outline were observed in the sample prepared from the  $0.10 \text{ mol dm}^{-3} \text{ Zn(NO}_3)_2$  solution on the ten-layered  $\text{TiO}_2$ . The increase in the  $\text{TiO}_2$  layer thickness increased the photocatalytic reduction rate of  $\text{NO}_3^-$  and formation rate of  $\text{OH}^-$ . This reaction causing the pH increase promoted the LZH formation.

### Figure 8

Figure 9 shows the XRD patterns of the samples prepared from the  $0.10$ ,  $0.30$  and  $0.50 \text{ mol dm}^{-3} \text{ Zn(NO}_3)_2$  solutions on the three-layered  $\text{TiO}_2$  and the sample prepared from the  $0.10 \text{ mol dm}^{-3} \text{ Zn(NO}_3)_2$  solution on the ten-layered  $\text{TiO}_2$ . The intensity of the XRD peaks due to the LZHs increased with an increase in the  $\text{Zn(NO}_3)_2$  concentration. The crystallite sizes of the LZH nitrate and ZnO for each sample were estimated from the XRD peaks and are shown in Table 1. The crystallite size of the LZH nitrate increased whereas the ZnO crystallite size decreased with an increase in the  $\text{Zn(NO}_3)_2$  concentration. No ZnO peak was observed in the sample prepared from the  $0.50 \text{ mol dm}^{-3} \text{ Zn(NO}_3)_2$  solution on the three-layered  $\text{TiO}_2$ . The intensity of the XRD peaks due to both the LZHs and ZnO increased by an increase in the  $\text{TiO}_2$  layer thickness. For the sample containing the ten-layered  $\text{TiO}_2$ , an anatase peak was observed at  $25.3^\circ$ . The increase in the  $\text{Zn(NO}_3)_2$  concentration caused the promotion of the LZH formation. The increase in the  $\text{TiO}_2$  layer thickness increased the formation rate of the

LZHs and their dehydration rate. Additionally, a peak was observed at  $12.3^\circ$ , which was suggested to be due to the Zn/Ti-layered double hydroxide (LDH) or Zn/Ti-NO<sub>3</sub>-LDH produced by the reaction between Zn(NO<sub>3</sub>)<sub>2</sub> and the TiO<sub>2</sub> film surface under basic conditions [23–25].

### Figure 9

The reaction temperature increased both the formation rate of the LZHS and their dehydration rate. Therefore, the ZnO crystals grew without crystal growth of the LZHS at high temperature. The TiO<sub>2</sub> film thickness also increased both rates, especially the formation rate of the LZHS. This resulted in a significant number of ZnO crystals and a small amount of LZH crystals at high temperature. Only the formation rate of LZHS increased based on the Zn(NO<sub>3</sub>)<sub>2</sub> concentration. The crystal growth of the LZHS led to the sheet or flake structure. The ZnO crystallite and particles sizes were determined by the balance of the two rates. The crystallite sizes decreased with an increase in the formation rate and the number of ZnO crystal nuclei. The microcrystals were formed on the parts on which the Ag or Pd were aggregated. The appropriate control of the reaction rates can provide a thin film consisting of only the nanocrystals which are preferable for photovoltaic electrodes.

## 4. Conclusions

The films consisting of the ZnO nanoparticles were prepared from an aqueous solution of  $\text{Zn}(\text{NO}_3)_2$  on the substrate plate with a very thin  $\text{TiO}_2$  film by a photocatalytic reaction. The influence of the reaction conditions on the microscopic morphology of the deposited particles and the mechanism of their formation were investigated based on the surface analyses of the samples. The amorphous or low crystalline LZH aggregates were deposited at 323 and 338 K. The ZnO crystals with about 1–2  $\mu\text{m}$ -sized hexagonal columns and 10 nm-sized spheres were formed at 338–358 K. Nitrate ions in the solution were reduced to nitrite ions, and water was transformed into hydroxide ions by the photocatalytic reaction on the  $\text{TiO}_2$  film. The pH value increased on the substrate surface with the  $\text{TiO}_2$  film, which caused the LZH formation on the film. The LZH was then dehydrated and transformed into ZnO. The average ZnO crystallite size decreased with an increase in the reaction temperature because the reaction rates of the formation and dehydration of the LZHs increased resulting in an increase in the formation rate of the ZnO crystal nuclei. The appropriate control of the reaction rates can provide a thin film consisting of only the nanocrystals.

### **Acknowledgements**

This work has been supported by JSPS KAKENHI Grant Number 24550153.

### **References**



- [1] L. Spanhel, M. A. Anderson, *J. Am. Chem. Soc.* 113 (1991) 2826–2833.
- [2] J. A. Anta, E. Guillén, R. Tena-Zaera, *J. Phys. Chem. C* 116 (2012) 11413–11425.
- [3] S. Sakthivel, B. Neppolian, M.V. Shankar, B. Arabindoo, M. Palanichamy, V. Murugesan, *Sol. Energy Mater. Sol. Cells* 77 (2003) 65–82.
- [4] M. Izaki, T. Omi, *Appl. Phys. Lett.* 68 (1996) 2439–2440.
- [5] S. Peulen, D. Lincot, *Adv. Mater.* 8 (1996) 166–170.
- [6] S. Peulen, D. Lincot, *J. Electrochem. Soc.* 145 (1998) 864–874.
- [7] M. Izaki, T. Omi, *J. Electrochem. Soc.* 144 (1997) L3–L5.
- [8] T. Shinagawa, K. Murase, S. Otomo, J. Katayama, M. Izaki, *J. Electrochem. Soc.* 156 (2009) H320–H326.
- [9] M. Izaki, J. Katayama, *J. Electrochem. Soc.* 147 (2000) 210–213.
- [10] M. Izaki, *Chem. Commun.* 2002, 476–477.
- [11] S. Nagaya, H. Nishikiori, *Chem. Lett.* 41 (2012) 993–995.
- [12] M. Izaki, *J. Electrochem. Soc.* 143 (1996) L53–L55.
- [13] S. Otani, J. Katayama, H. Umemoto, M. Matsuoka, *J. Electrochem. Soc.* 153 (2006) C551–C556.
- [14] Y. Masuda, K. Kato, *Cryst. Growth Des.* 8 (2008) 275–279.
- [15] W. Lu, H. Schmidt, *Adv. Powder Technol.* 19 (2008) 1–12.

- [16]S. Nagaya, H. Nishikiori, ACS Appl. Mater. Interfaces 5 (2013) 8841–8844.
- [17]G. G. C. Arizaga, A. S. Mangrich, J. E. F. C. Gardolinski, F. Wypych, J. Colloid Interface Sci. 320 (2008) 168–176.
- [18]H. Bae, H. Jung, Bull. Korean Chem. Soc. 33 (2012) 1949–1954.
- [19]P. Li, Z. P. Xu, M. A Hampton, D. T. Vu, L. Huang, V. Rudolph, A. V Nguyen, J. Phys. Chem. C 116 (2012) 10325–10332.
- [20]A. F. Abdul Latip, M. Z. Hussein, J. Stanslas, C. C. Wong, R. Adnan, Chem. Central J. 7:119 (2013) 1–11.
- [21]B. Tansel, J. Sager, T. Rector, J. Garland, R. F. Strayer, L. Levine, M. Roberts, M. Hummerick, J. Bauer, Sep. Purif. Technol. 51 (2006) 40–47.
- [22]L. J. Banasiak, A. I. Schäfer, J. Membr. Sci. 334 (2009) 101–109.
- [23]M. Shao, J. Han, M. Wei, D. G. Evans, X. Duan, Chem. Eng. J. 168 (2011) 519–524.
- [24]S. J. Xia, F. X. Liu, Z. M. Ni, J. L. Xue, P. P. Qian, J. Colloid Interface Sci. 405 (2013) 195–200.
- [25]S. J. Xia, F. X. Liu, Z. M. Ni, W. Shi, J. L. Xue, P. P. Qian, Appl. Catal. B: Environ. 144 (2014) 570–579.

**Table 1** Average crystallite sizes of  $\text{Zn}_5(\text{OH})_8(\text{NO}_3)_2 \cdot 6\text{H}_2\text{O}$  and ZnO for the samples prepared from the solutions with different concentrations of  $\text{Zn}(\text{NO}_3)_2$  on the three- and ten-layered  $\text{TiO}_2$ .

$\text{Zn}(\text{NO}_3)_2$ concentration / $\text{mol dm}^{-3}$	0.10	0.30	0.50	0.10
Number of $\text{TiO}_2$ layer	3	3	3	10
Crystallite size / nm				
$\text{Zn}_5(\text{OH})_8(\text{NO}_3)_2 \cdot 6\text{H}_2\text{O}$	-	18.2	28.2	29.2
ZnO	35.7	25.2	-	29.2

## Figure captions

**Figure 1** Secondary electron images by SEM observations of the sample surface prepared on the substrate plates at (a) 323, (b) 338, (c) 348, and (d) 358 K.

**Figure 2** XRD patterns of the sample surface prepared on the substrate plates at (1) 323, (2) 338, (3) 348, and (4) 358 K.

**Figure 3** EPMA mapping images of the sample prepared at 348 K.

**Figure 4** Reflection electron images of SEM (a) on the surface and (b) at the cross section of the sample prepared at 348 K.

**Figure 5** EDS mapping images of STEM at (a) the microcrystal and (b) thin film parts of the sample prepared at 348 K.

**Figure 6** TEM image of the cross section of the sample prepared at 348 K.

**Figure 7** (a) UV-vis absorption and (b) IPCE spectra of (1) the substrate coated with TiO<sub>2</sub> layer and the samples prepared at (2) 323, (3) 338, (4) 348, and (5) 358 K.

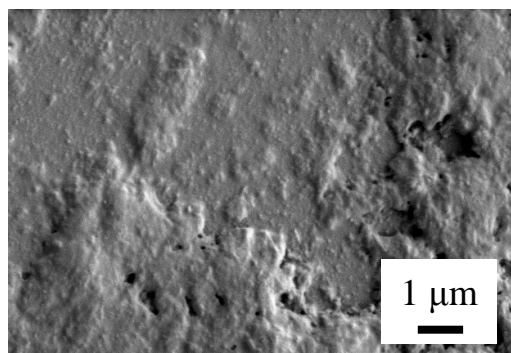
**Figure 8** SEM images of the samples prepared from (a) the 0.30 and (b) 0.50 mol dm<sup>-3</sup> Zn(NO<sub>3</sub>)<sub>2</sub> solutions on the three-layered TiO<sub>2</sub> and (c) the sample prepared from the 0.10 mol dm<sup>-3</sup> Zn(NO<sub>3</sub>)<sub>2</sub> solution on the ten-layered TiO<sub>2</sub>.

**Figure 9** XRD patterns of the samples prepared from (1) the 0.10, (2) 0.30 and (3) 0.50 mol

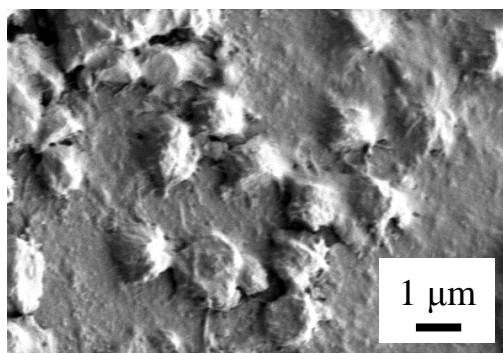
$\text{dm}^{-3} \text{Zn}(\text{NO}_3)_2$  solutions on the three-layered  $\text{TiO}_2$  and (4) the sample prepared from the  $0.10 \text{ mol dm}^{-3} \text{Zn}(\text{NO}_3)_2$  solution on the ten-layered  $\text{TiO}_2$ .

**Figure 1**

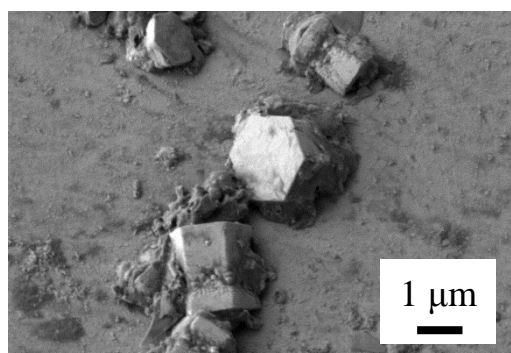
(a)



(b)



(c)



(d)

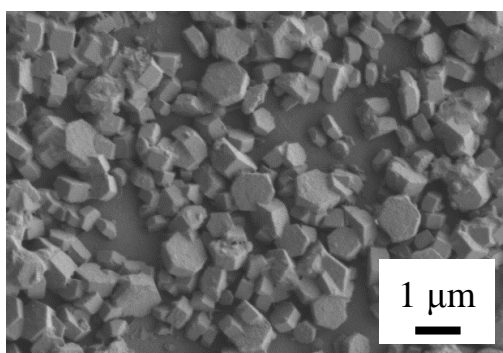
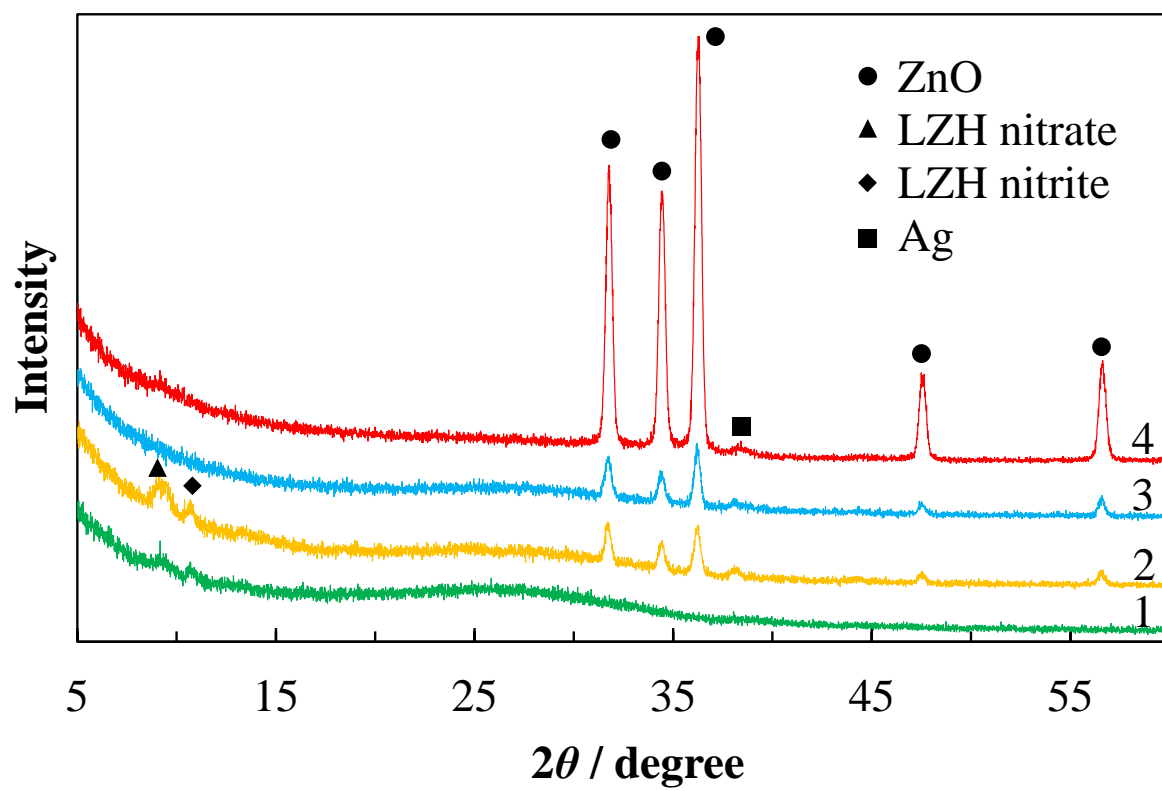
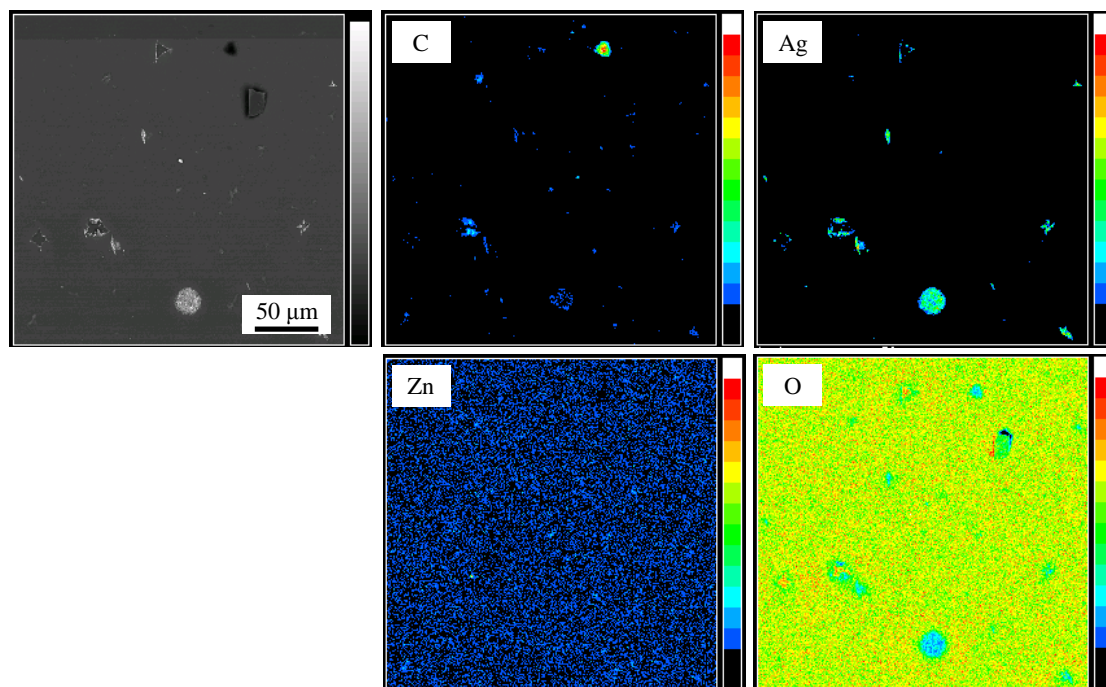


Figure 2



**Figure 3**

(a)



(b)

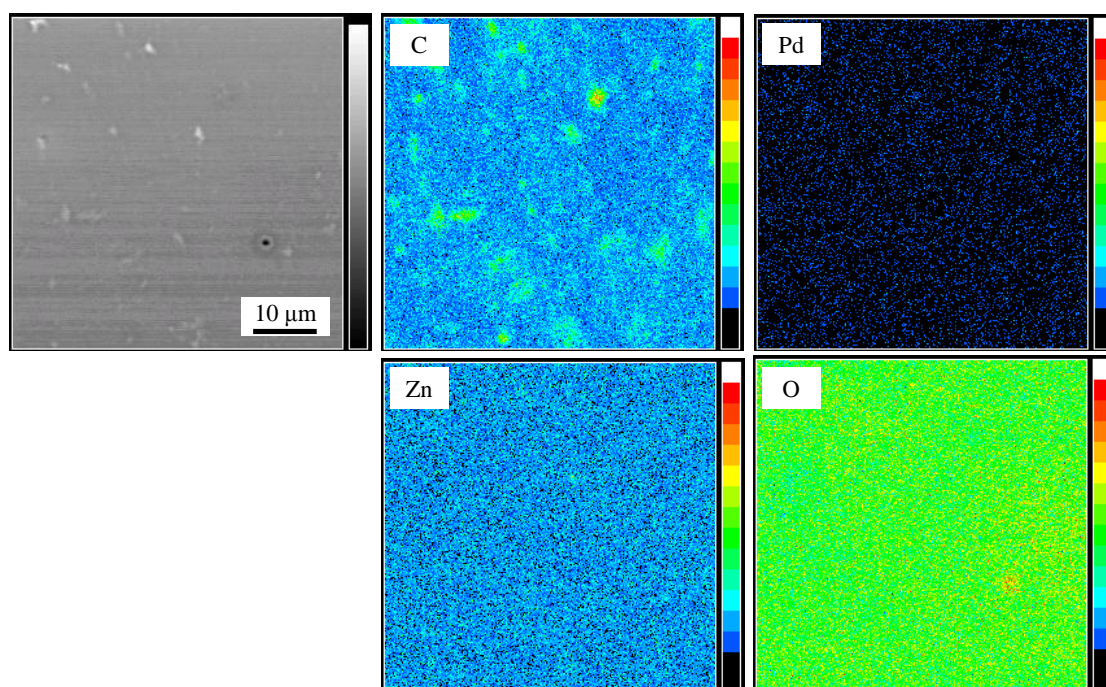
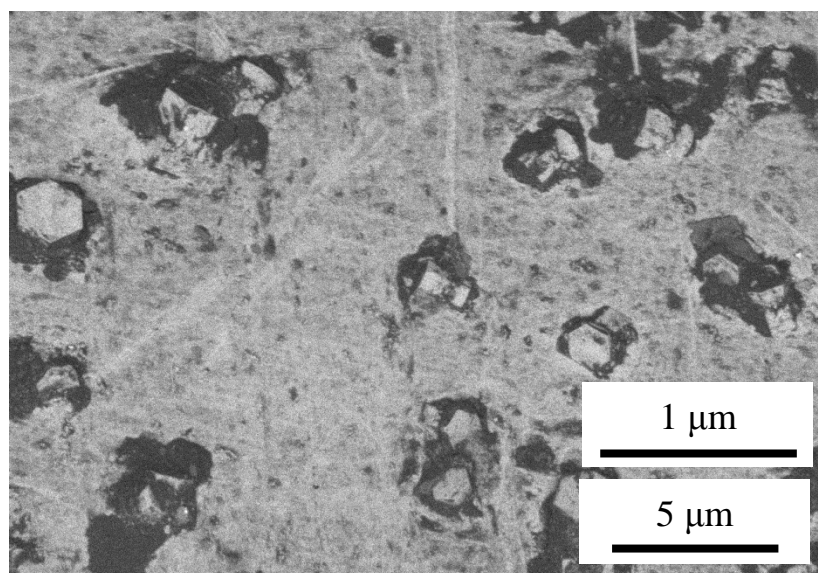




**Figure 4**

(a)



(b)

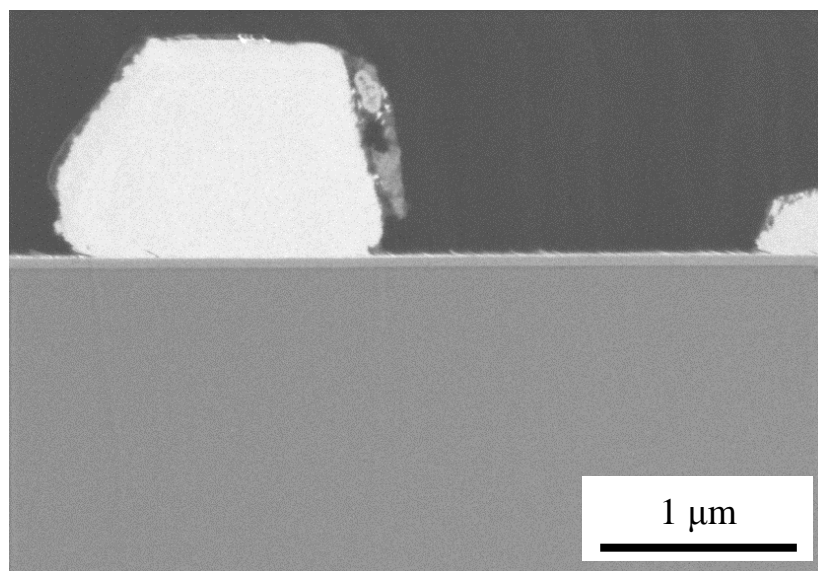
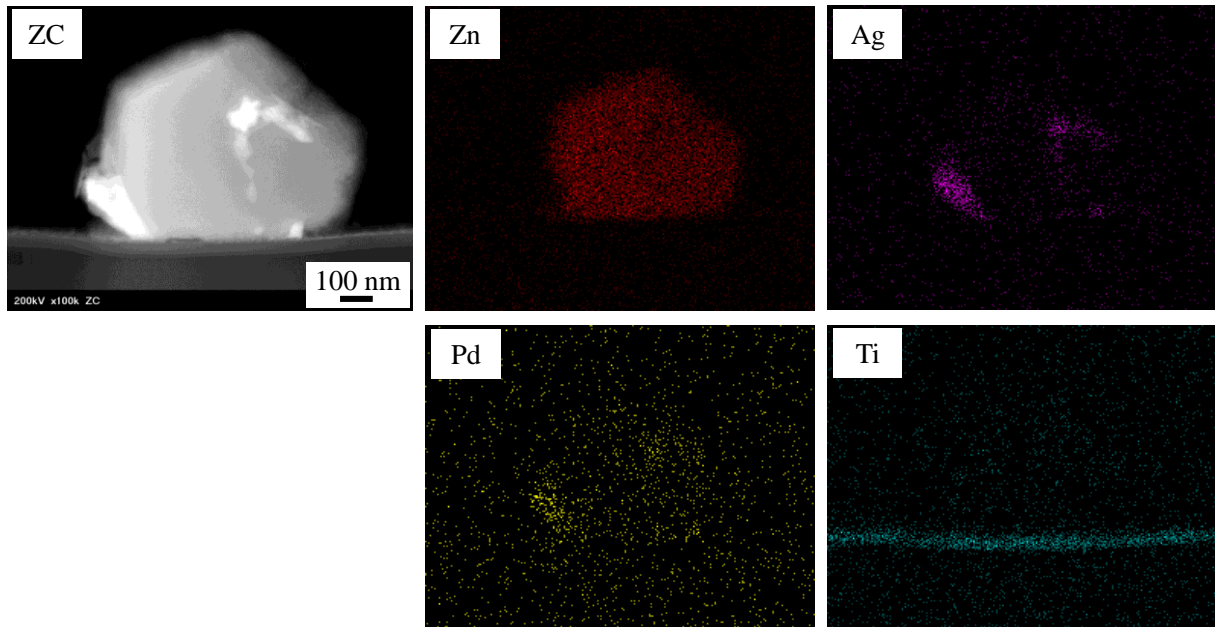


**Figure 5**

(a)



(b)

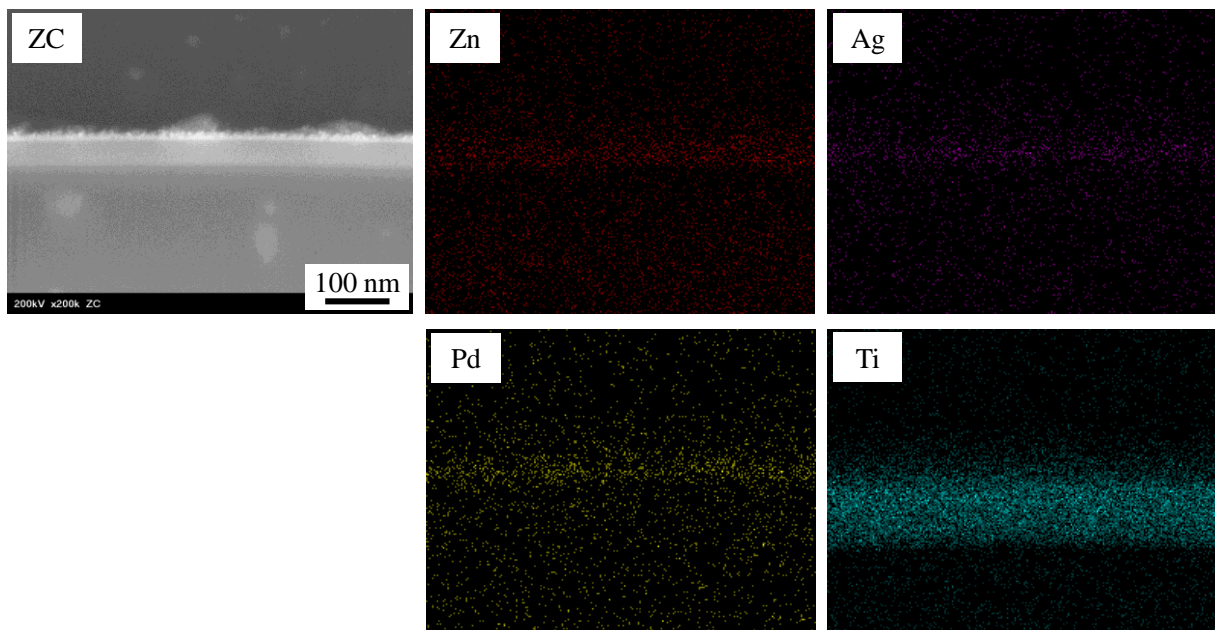


**Figure 6**

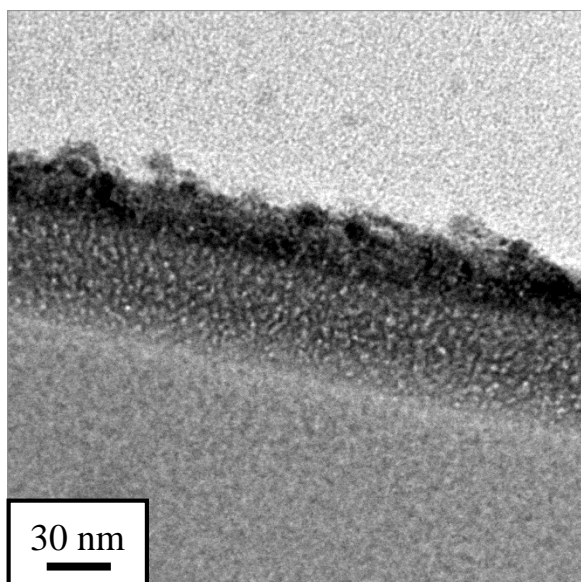
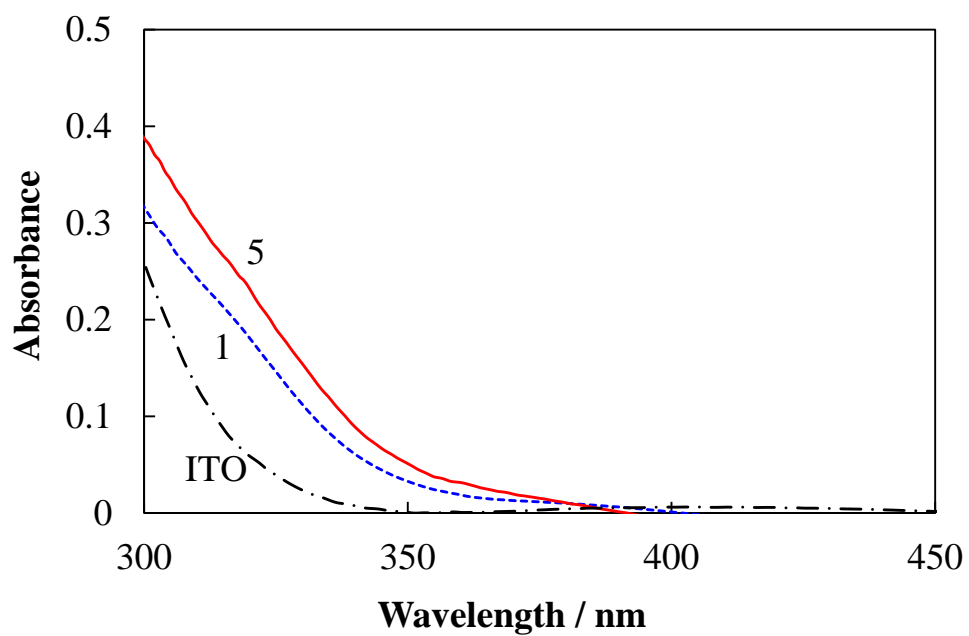


**Figure 7**

(a)



(b)

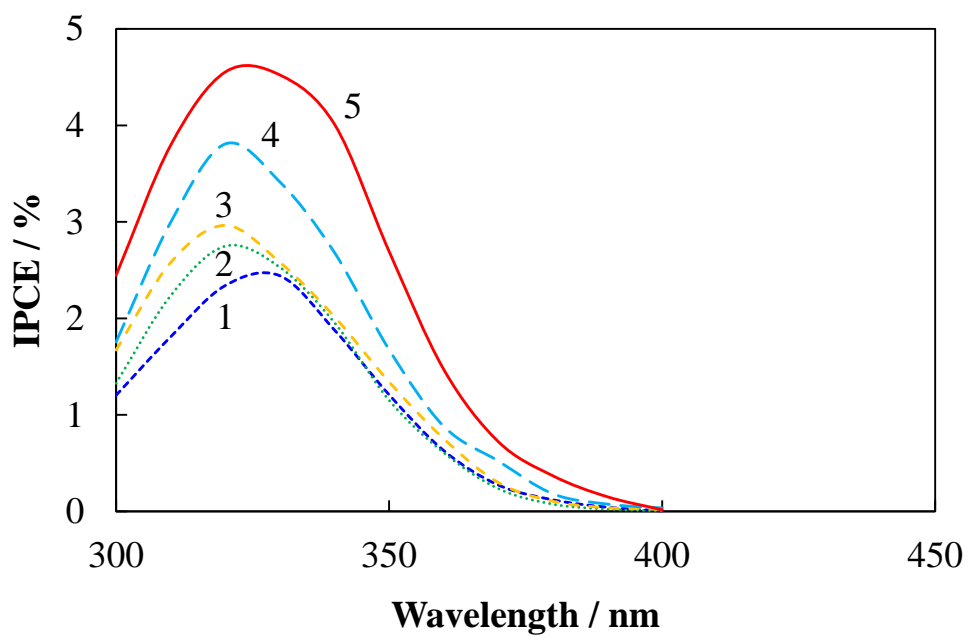
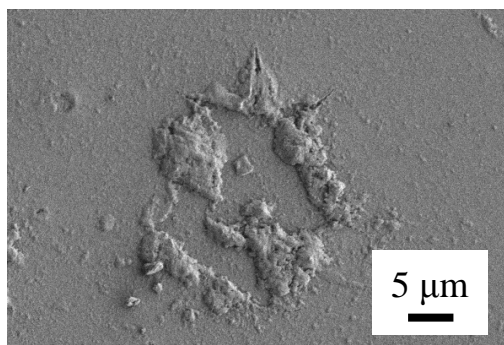
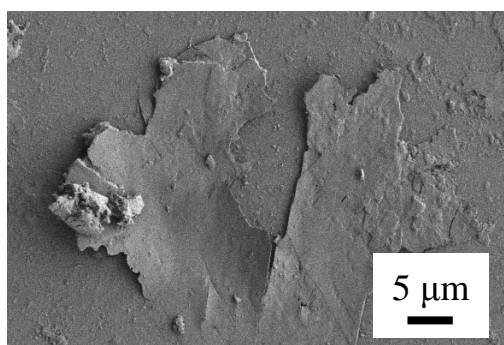


**Figure 8**

(a)



(b)



(c)

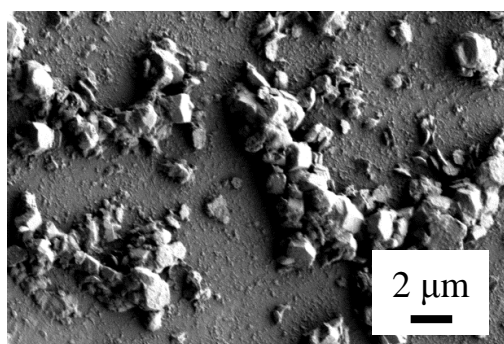


Figure 9

